Phase Evolution and Magnetic Characteristic of $Fe_{64}Co_{16}Zr_{10}B_{10}$ Amorphous Alloy

Zhong Hua[a,*], Taotao Feng[a], Yuecheng Wu[a], Wanqiu Yu[b] and Yaodi Liu[b]

[a] *General Education Center, Quanzhou University of Information Engineering, 362000 Quanzhou, China*
[b] *College of Physics, Jilin Normal University, 136000 Siping, China*

Received: 07.04.2022 & Accepted: 25.02.2022

Doi: 10.12693/APhysPolA.141.630 *e-mail: hz196110@126.com

$Fe_{64}Co_{16}Zr_{10}B_{10}$ amorphous alloy prepared by a single roller melt spinning was annealed under isothermal treatment at temperatures ranging from 550 to 650°C in a vacuum. Phase evolution and magnetic characteristic of $Fe_{64}Co_{16}Zr_{10}B_{10}$ amorphous alloy were investigated in detail by combining X-ray diffraction, transmission electron microscopy, scanning transmission electron microscopy/energy dispersive spectroscopy, and vibrating sample magnetometer. At 550°C, the metastable intermediate α-Mn type phase precipitates, as well as an α-Fe(Co) phase. At 575°C, only metastable α-Mn type phase is observed. Scanning transmission electron microscopy/energy dispersive spectroscopy indicates that the α-Mn type nanocrystals contain Fe, Co, and Zr. More Zr is at the interface between the nanocrystals and the amorphous matrix. There is little change in Co concentration among the remaining amorphous matrix, the nanocrystals, and the interface between the nanocrystals and the amorphous matrix. With a further increase in annealing temperature, the crystallization volume fraction of the α-Mn type phase decreases, and the crystallization volume fraction of the α-Fe(Co) phase increases accordingly. Coercivity of $Fe_{64}Co_{16}Zr_{10}B_{10}$ alloy undergoes a sharp rise above 550°C and a sharp decline above 600°C.

topics: amorphous, crystallization, phase evolution, magnetic property

1. Introduction

With the development of material science, the discovery and application of many metastable phase materials [1–9] make the formation and characteristics of the metastable phase one of the scientific and technological interests. The metastable phase of alloy materials has always been a hot and frontier issue in material science research. Researchers are committed to identifying metastable phases in some of the alloy materials and the influence of metastable phases on the properties of alloy materials.

Fe-based nanocrystalline soft magnetic alloys, as important functional materials, have widely attracted attention. Over the past several decades, during the primary crystallization of Fe-based amorphous alloys, different kinds of metastable phases have been reported, such as $Fe_{23}B_6$ type [10–13], $Fe_{12}Si_2ZrB$ type [14, 15], β-Mn type [16, 17] and α-Mn type (χ) [18–22], χ-FeCrMo-like structure [23] and $Nb_5Fe_{33}B_{10}$ phases [24]. The α-Mn type phase is the most common primary metastable phase in Fe-based alloys.

Our research group has reported some metastable phases precipitated in Fe-based alloys [14, 17, 25–27]. On the basis of our previous research, we choose $Fe_{64}Co_{16}Zr_{10}B_{10}$ alloy as the research object. For $Fe_{64}Co_{16}Zr_{10}B_{10}$ alloy, we found that the faster the heating rate is, the higher the content of the α-Mn type phase is [27]. However, the distribution proportions of Fe, Co and Zr in the remaining amorphous matrix, the α-Mn type nanocrystal, and the interface between the nanocrystal and the amorphous matrix, are still unclear. The phase evolution of this alloy in detail and the corresponding magnetic characteristics need to be further studied.

2. Experimental details

The ingot with a nominal composition of $Fe_{64}Co_{16}Zr_{10}B_{10}$, prepared by arc melting with the mixtures of high pure elements (99.98 wt% Fe, 99.99 wt% Co, 99.92 wt% Zr, 99.99 wt% B), was remelted four times with magnetic stirring in a high purity argon atmosphere to ensure its homogeneity. The corresponding ribbon was prepared by

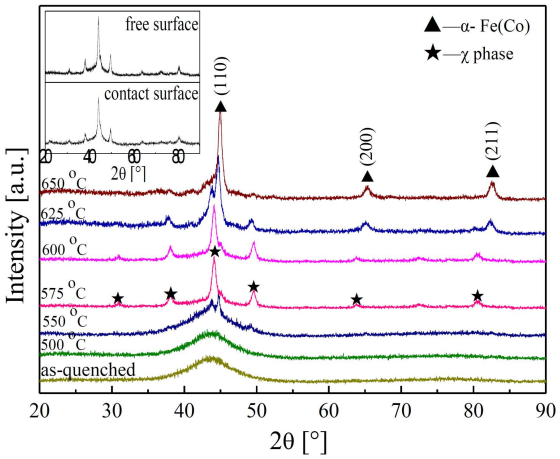

Fig. 1. XRD patterns of $Fe_{64}Co_{16}Zr_{10}B_{10}$ alloys as-quenched and annealed at different temperatures. The insert gives the XRD patterns of alloy annealed at 575°C taken by the free surface and the wheel contact surface.

a single roller melt spinning and rapidly isothermally annealed at 500, 550, 575, 600, 625, and 650°C for 40 min in a vacuum. The copper-wheel rate is 38 m/s. Structural characterizations of alloys were measured by X-ray diffraction (XRD)(D/max 2500/PC, Cu K_α, $\lambda = 1.5406$ Å, 40 kV, 200 mA, scan speed: 4 deg/min) and transmission electron microscopy (TEM)(FEI Talos F200). Fischione Model 1050 TEM Mill was used to prepare TEM samples. Scanning transmission electron microscopy/energy dispersive spectroscopy (STEM-EDS) was used to observe the element concentration. Coercivity (H_c) was determined by a vibrating sample magnetometer (VSM)(Lake Shore M7407).

3. Results and discussion

XRD patterns of $Fe_{64}Co_{16}Zr_{10}B_{10}$ alloys as-quenched and annealed at 500, 550, 575, 600, 625, and 650°C taken by the free surface are shown in Fig. 1. $Fe_{64}Co_{16}Zr_{10}B_{10}$ alloy as-quenched is in an amorphous state. When the alloy is annealed at 550°C, both α-Fe(Co) and α-Mn type (χ-phase) crystallization phases precipitate from the amorphous matrix. However, when the alloy is annealed at 575°C, a single metastable intermediate α-Mn type phase can be seen.

The insert in Fig. 1 shows the XRD patterns of the alloy annealed at 575°C, taken by both the free surface and the wheel contact surface. There is little difference between the structure of the free surface and the wheel contact surface. In the single roller melt spinning technique, there is a cooling gradient in the cross-section direction of the ribbon during the preparation processing. The cooling speed of the wheel contact surface is greater than that of the free surface, and there are some differences in the structures of the two sides of the ribbon. The

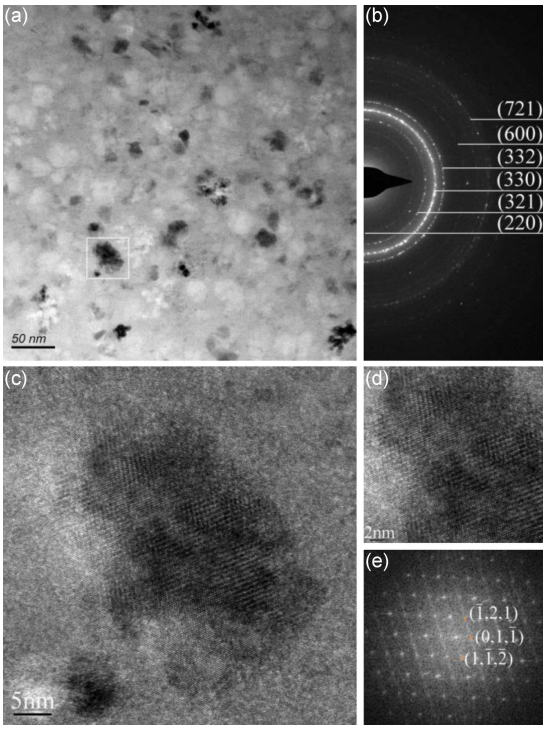

Fig. 2. TEM image, SAED pattern (a, b), HRTEM images (c, d), and FFT (e) of $Fe_{64}Co_{16}Zr_{10}B_{10}$ alloy annealed at 575°C.

magnitude of this difference also varies for different alloys and different preparation parameters. From the results of XRD tests, the difference is slight for the $Fe_{64}Co_{16}Zr_{10}B_{10}$ alloy ribbon prepared in this paper. Previous studies by our research group have shown that when thermal energy provided by heat treatment overcomes the nucleation barrier of the χ-phase, the χ-phase preferentially nucleates instead of the α-Fe phase [25]. Therefore, when the alloy is annealed at 575°C, the crystalline phase is only the χ-phase. The intermediate χ-phase is metastable and transforms into α-Fe solid solution with an increase in annealing temperature. There is little of α-Mn type at 650°C and a lot of α-Fe(Co). The diffraction peaks of α-Fe(Co) shift to a high angle, and the corresponding lattice constant of α-Fe(Co) is 2.8538(3) Å. The lattice constant of pure α-FeCo is 2.8550 Å, indicating that some B atoms also dissolve into α-Fe(Co).

Figure 2 shows the transmission electron microscope (TEM) image, the corresponding selected area electron diffraction (SAED) pattern, the high resolution transmission electron microscope (HRTEM) images, and the corresponding fast Fourier transforms (FFT) of $Fe_{64}Co_{16}Zr_{10}B_{10}$ alloy annealed at 575°C. The nanocrystals distribute into the remained amorphous matrix, exhibiting different sizes and irregular shapes. The grain size ranges from 10 to 50 nm. The planes of the α-Mn phase are marked in the electron diffraction pattern. No other phase was observed. The HRTEM

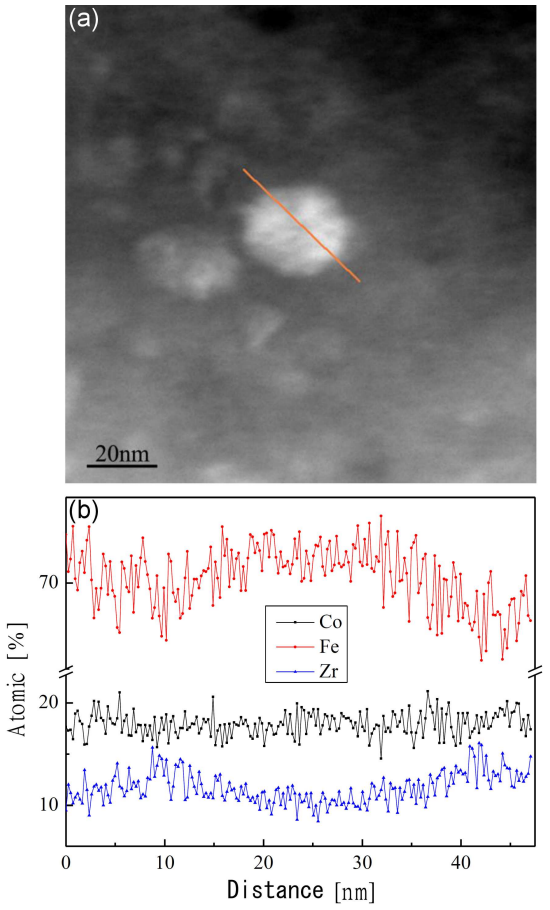

Fig. 3. TEM image (a) and STEM-EDS line-scan (b) of α-Mn type phase nanocrystal.

images (c, d) and FFT (e) of the selected grain are given. The DigitalMicrograph software was used to index diffraction spots. It was determined that the grain is α-Mn type grain. The corresponding zone axis is [311].

The results of the STEM-EDS line-scan of α-Mn type nanocrystal are shown in Fig. 3. The nanocrystal, the residual amorphous matrix, and the interface between the nanocrystal and the remaining amorphous matrix all contain Fe, Co, and Zr. There is little change in Co concentration between the nanocrystal and the remaining amorphous matrix. The content of Zr is higher, and the content of Fe is lower in the interface between the nanocrystal and the amorphous matrix compared with the nanocrystal and the remaining amorphous matrix. The ratio of Fe:Co:Zr in the intermediate region of the grain is about 72:18:10, and in the nominal component it is 64:16:10. The ratio of Co and Zr in the intermediate region of the grain is close to that in the nominal component value. The ratio of Fe in the intermediate region is higher.

Figure 4 shows the transmission electron microscope image, the corresponding selected-area electron diffraction pattern, and the high resolution transmission electron microscope images of

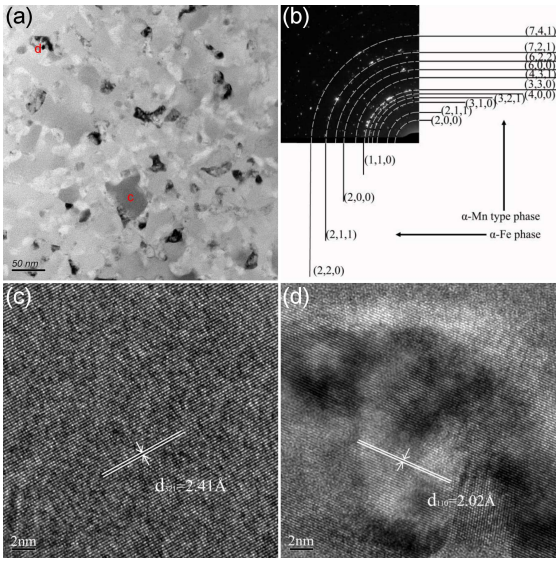

Fig. 4. TEM image (a), SAED pattern (b), and HRTEM images (c, d) of $Fe_{64}Co_{16}Zr_{10}B_{10}$ alloy annealed at 625°C.

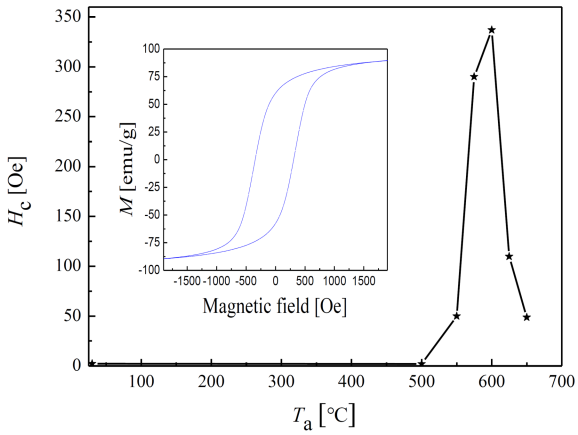

Fig. 5. Coercivity (H_c) of $Fe_{64}Co_{16}Zr_{10}B_{10}$ alloy as a function of temperature. The insert shows the hysteresis loop of alloy annealed at 600°C.

$Fe_{64}Co_{16}Zr_{10}B_{10}$ alloy annealed at 625°C. The nanocrystals exhibit irregular shapes. The planes of the α-Fe(Co) phase and α-Mn type phase are marked in the electron diffraction pattern. The HRTEM images of grain c and grain d are shown in Fig. 4c and d, respectively. The interplanar spacing is 2.41 Å and 2.02 Å, which corresponds to the (321) plane of the α-Mn type phase and the (110) plane of the α-Fe(Co) phase, respectively.

Figure 5 shows the coercivity(H_c) of $Fe_{64}Co_{16}Zr_{10}B_{10}$ alloy as a function of annealing temperature (T_a). It is worth noting that H_c undergoes a sharp rise above 550°C and a sharp decline above 600°C, which is closely related to their microstructure. After annealing at 600°C, H_c reaches the maximum, whose crystallization product contains a lot of α-Mn type phase. The α-Mn

type phase is a metastable semi-hard magnetic phase. As annealing temperature increases, H_c decreases continuously, accompanied by the vanishing of the α-Mn type phase.

4. Conclusions

$Fe_{64}Co_{16}Zr_{10}B_{10}$ amorphous alloy was annealed under isothermal treatments in a vacuum. Phase evolution and magnetic characteristic of $Fe_{64}Co_{16}Zr_{10}B_{10}$ alloy are investigated in detail.

1. At 550°C, the metastable intermediate α-Mn type phase precipitates as well as the α-Fe(Co) phase. At 575°C, only metastable α-Mn type phase is observed. With the increase in annealing temperature, the crystallization volume fraction of the α-Mn type phase decreases, and the crystallization volume fraction of α-Fe(Co) phase increases accordingly.
2. The nanocrystal, the residual amorphous matrix, and the interface between the nanocrystal and the amorphous matrix all contain Fe, Co, and Zr. There is little change in Co concentration between the nanocrystal and the remaining amorphous matrix. The content of Zr is higher, and the content of Fe is lower in the interface between the nanocrystal and the amorphous matrix compared with the nanocrystal and the remaining amorphous matrix.
3. Coercivity (H_c) of $Fe_{64}Co_{16}Zr_{10}B_{10}$ alloy undergoes a sharp rise above 550°C and a sharp decline above 600°C.

Acknowledgments

This work was supported by the Technology Studying Project of the Office of Education of Jilin Province (No. JJKH20210451KJ) and the Sinoma Institute of Materials Research (Guang Zhou) Co., Ltd.

References

[1] J. Zhang, Y.J. Li, W. Li, *J. Mater. Sci.* **56**, 11456 (2021).

[2] C.Q. Liu, H.W. Chen, M. Song, J.F. Nie, *J. Mater. Sci. Technol.* **84**, 133 (2021).

[3] J.W. Wang, L. Liu, K.X. Yu, H.Z. Bai, J. Zhou, W.H. Zhang, X.R. Hu, G.P. Tang, *Int. J. Mol. Sci.* **21**, 9213 (2020).

[4] Y. Liu, W.M. Wang, H.D. Zhang, H.J. Ma, B. An, *J. Mater. Sci. Technol.* **28**, 1102 (2012).

[5] V. Rangelova, T. Spassov, *J. Alloys Compd.* **345**, 148 (2002).

[6] M. Glatt, H. Hotz, P. Kölsch, A. Mukherjee, B. Kirsch, J.C. Aurich, *Int. J. Adv. Manuf. Technol.* **115**, 749 (2021).

[7] S. Shukla, A.P. Patil, *Procedia Struct. Integ.* **14**, 259 (2019).

[8] Y.T. Wu, M.L. Li, X.F. Wang, L.L. Wang, H. Gao, *Mater. Manuf. Processes* **32**, 480 (2016).

[9] Y.T. Wu, M.L. Li, J. Yuan, X.F. Wang, *Appl. Phys. A* **123**, 543 (2017).

[10] A. Hirata, Y. Hirotsu, K. Amiya, N. Nishiyama, A. Inoue, *Phys. Rev. B* **80**, 140201 (2009).

[11] M. Nabiałek, B. Jeż, K. Błoch, *Metall. Mater. Trans. A* **51**, 4602 (2020).

[12] P. Svec, P. Svec Sr., J. Hosko, D. Janickovic, *J. Alloys Compd.* **590**, 87 (2014).

[13] T. Hibino, T. Bitoh, *J. Alloys Compd.* **707**, 82 (2017).

[14] X.Y. Xiong, T.R. Finlayson, B. C. Muddle, *J. Mater. Sci.* **38**, 1161 (2003).

[15] X.Y. Xiong, B.C. Muddle, T.R. Finlayson, *J. Phys. D: Appl. Phys.* **36**, 223 (2003).

[16] T.A. Velikanova, M.V. Karpets, *Powder Metall. Met. Ceram.* **50**, 479 (2011).

[17] W.Q. Yu, L.P. Lu, B. Zuo, Z. Hua, G.L. Xing, X.Y. Wang, D.D. Wang, *Appl. Phys. A* **125**, 636 (2019).

[18] T. Nagase, Y. Umakoshi, *ISIJ Int.* **46**, 1371 (2006).

[19] Y.C. Chen, C.M. Chen, K.C. Su, K. Yang, *Mat. Sci. Eng. A* **133**, 596 (1991).

[20] I.V. Lyasotsky, N.B. Dyakonova, D.L. Dyakonov, *J. Alloys Compd.* **586**, S20 (2014).

[21] I.V. Lyasotsky, N.B. Dyakonova, D.L. Dyakonov, E.N. Vlasova, M.Y. Jazvitsky, *Rev. Adv. Mater. Sci.* **18**, 695 (2008).

[22] M. Imafuku, S. Sato, H. Koshiba, E. Matsubara, A. Inoue, *Scr. Mater.* **44**, 2369 (2001).

[23] A. Hirata, Y. Hirotsu, K. Amiya, A. Inoue, *Phys. Rev. B Condens. Matter* **79**, 020205 (2009).

[24] T.A. Sviridova, T.R. Chueva, M.V. Gorshenkov, E.V. Shelekhov, P.A. Borisova, *J. Alloys Compd.* **658**, 525 (2015).

[25] Y.M. Sun, B. Zuo, D. Wang, X.C. Meng, *Acta Phys. Pol. A* **124**, 685 (2013).

[26] W.Q. Yu, Q.L. Zhou, Z.S. Liu, H.Q. Zeng, Z.Q. Wang, Z. Hua, *J. Mater. Eng. Perform.* **26**, 4807 (2017).

[27] W.Q. Yu, H.Q. Zeng, Y.M. Sun, Y.J. Sun, Z. Hua, *Phys. Lett. A* **381**, 1573 (2017).